Dynamic multilevel multiscale simulation of naturally fractured reservoirs with generic fracture-matrix conductivity contrasts

HosseiniMehr, Mousa; Al Kobaisi, Mohammed; Vuik, Cornelis; Hajibeygi, Hadi

DOI
10.2118/196626-MS

Publication date
2019

Document Version
Final published version

Published in
Society of Petroleum Engineers - SPE Reservoir Characterisation and Simulation Conference and Exhibition 2019, RCSC 2019

SPE-196626-MS

Dynamic Multilevel Multiscale Simulation of Naturally Fractured Reservoirs with Generic Fracture-Matrix Conductivity Contrasts

Mousa HosseiniMehr, Department of Applied Mathematics, TU Delft, Delft, Netherlands; Mohammed Al Kobaisi, Department of Petroleum Engineering, Khalifa University of Science and Technology; Cornelis Vuik, Department of Applied Mathematics, TU Delft, Delft, Netherlands; Hadi Hajibeygi, Department of Geoscience and Engineering, TU Delft, Delft, Netherlands

This paper was prepared for presentation at the SPE Reservoir Characterisation and Simulation Conference and Exhibition held in Abu Dhabi, UAE, 17 - 19 September 2019.

Abstract

An algebraic dynamic multilevel (ADM) method for multiphase flow in heterogeneous fractured porous media using the projection-based embedded discrete fracture model (pEDFM) is presented. The fine-scale discrete system is obtained independently for matrix and each lower-dimensional fracture. On the fine-scale high resolution computational grids, an independent dynamic multilevel gird (i.e., ADM grid) is imposed. The fully implicit discrete system is mapped completely algebraically to this ADM grid resolution using sequences of restriction and prolongation operators. Multilevel multiscale basis functions are locally computed and employed to honor the heterogeneity contrasts of the fractured domain by interpolating the solution accurately. These basis functions are computed only at the beginning of the simulation to increase the computational efficiency. Once the ADM system is solved for all unknowns (i.e., pressure and saturation), the solution at ADM resolution is prolonged back to fine-scale resolution in order to obtain an approximated fine-scale solution. This dynamic multilevel system employs the fine-scale grid cells only at the sharp gradient of the solution (e.g., at the moving front). With two fractured test-cases (homogeneous and heterogeneous), the performance of ADM is assessed by comparing it to fine-scale results as reference solution. It will be shown that ADM is able to reduce the computational costs and provide efficiency while maintaining the desired accuracy.

Introduction

In majority of geoscience and geoengineering applications, multiphase fluid flow in porous media with complex physical phenomena is involved from small to large scales (from orders of millimeters up to kilometers). Accurate, scientific and scalable modelling of such physical phenomena are of great importance to satisfy the societal expectations on many different aspects (e.g., economical, environmental, etc.) of field development plans. To achieve this, the simulation models should be able to capture high contrasts in rock and fluid properties accurately, while providing scalability. Additionally, many reservoirs consist of

complex geological fracture networks with extensive conductivity contrasts which have heavy impacts on flow patterns. Therefore, rigorous representation of the fluid flow model in presence of these conductivity contrasts is paramount [1]. However, accomplishing this task introduces a number of computational challenges. The large size of the heterogeneous domain demands for high resolution computational grids [2]. Non-linear behavior due to strong coupling (e.g., capillarity) results in stability and convergence issues. Presence of fractures and faults with broad range of conductivity contrasts brings more bounding limits to the system. The geomechanical effects adds to the complexity [3], [4]. All the mentioned challenges demand for developing advanced simulation models that are capable of providing efficiency and scalability while maintaining desirable accuracy such that acceptable representation of the physical phenomena in fractured porous media is achievable[5].

In this article, an advanced scalable simulation method for multiphase fluid flow in fractured porous media is presented. Fully-implicit (FIM) method is used to ensure stability of non-linear behavior due to flow and transport coupling. As a more comprehensive approach compared to embedded discrete fracture model (EDFM) [6], [7], [8], projection-based EDFM (pEDFM) is employed to explicitly represent the fractures (with any range of conductivity contrast towards the rock matrix) [9]. The pEDFM implementation has been extended to include a fully 3D geometry. The fine-scale discretization is done for matrix and fractures independently. The main two unknowns are pressure and saturation of the flooding phase. Once the fine-scale discretized system is obtained using pEDFM, it is mapped to a dynamic multilevel grid (i.e., ADM grid) which is constructed based on hierarchically nested and multilevel coarse grids [10], [11], [12]. The mapping process is done fully algebraically where sequences of restriction (R) and prolongation (P) operators are used to map across multiple coarsening levels. Locally computed basis functions are employed to interpolate the solution at coarse levels [13], [14], [15]. To honor the heterogeneity of the domain, multiscale finite volume basis functions are used as pressure interpolators [16], [17], [18], [19], [20]. These basis functions are only computed at the beginning of the simulation providing computational efficiency. Once the system is solved at ADM resolution, it is mapped back to fine-scale resolution using prolongation operators. ADM allows for employing only a fraction of fine-scale grid cells only where and when it is needed using a front tracking technique, providing significant reduction in the number of degrees of freedom (DOF).

The article is organized as follows: the governing equations and fine-scale discretization is explained in section 2; ADM methodology is described in section 3; section 4 contains the numerical results, and lastly the article is concluded with section 5.

Governing Equations and Fine-scale Discretization

The mass balance equation in porous media for phase α, assuming no capillarity and gravity, with n_{frac} discrete fractures reads

$$\frac{\partial}{\partial t}\left(\phi^m \rho_\alpha^m S_\alpha^m\right) - \nabla\cdot\left(\rho_\alpha^m \lambda_\alpha^m \quad \nabla p^m\right) = \rho_\alpha^m q_\alpha^{mw} + \sum_{i=1}^{n_{frac}} \rho_\alpha^* Q_\alpha^{mf_i} \qquad on \quad \Omega_m \subseteq R^n$$

for the rock matrix m and

$$\frac{\partial}{\partial t}\left(\phi^{f_i} \rho_\alpha^{f_i} S_\alpha^{f_i}\right) - \nabla\cdot\left(\rho_\alpha^{f_i} \lambda_\alpha^{f_i} \nabla p^{f_i}\right) = \rho_\alpha^{f_i} q_\alpha^{f_i w} + \rho_\alpha^* Q_\alpha^{f_i m} + \left(\sum_{j=1}^{n_{frac}} \rho_\alpha^* Q_\alpha^{f_i f_j}\right)_{j\neq i} \qquad on \quad \Omega_{f_i} \subseteq R^{n-1}$$

for the lower dimensional fracture f_i. The superscripts m, f and w refer to matrix, fractures and wells, respectively. Subscript α denotes the phase index. ϕ is the porosity of the medium. ρ_α, S_α and λ_α are, the density, saturation, and mobility of phase α, respectively. $\lambda_\alpha = \frac{k_{r\alpha}}{\mu_\alpha} K$, where k_r and μ_α are the relative

permeability and viscosity of phase α. $\boldsymbol{K}$ is the permeability tensor (in case of anisotropy). q_α is the source term related to wells. $Q_\alpha^{mf_i}$ and $Q_\alpha^{f_i m}$ are the flux transfers between matrix and fracture for each phase α. $Q_\alpha^{f_i f_j}$ refers to flux transfer of phase α from fracture f_j to fracture f_i where intersection occurs. Due to conservation of mass, $\iiint_V Q^{mf_i} dV = -\iint_{Af_i} Q^{f_i m} dA$ and $\iint_{Af_i} Q^{f_i f_j} dA = -\iint_{Af_j} Q^{f_j f_i} dA$ applies. Peaceman's well model is used to formulate the source terms q_α^{mw} and $q_\alpha^{f_i w}$, namely

$$q_\alpha^{mw} = \frac{PI \cdot \lambda_\alpha^* \cdot (p^w - p^m)}{V} \quad , \qquad q_\alpha^{f_i w} = \frac{PI \cdot \lambda_\alpha^* \cdot (p^w - p^m)}{A} \quad ,$$

where, PI is the well productivity index and λ_α* is the effective mobility obtained between the source term and each medium. The matrix-fracture and fracture-fracture flux transfers (i.e., $Q_\alpha^{mf_i}$, $Q_\alpha^{f_i m}$ and $Q_\alpha^{f_i f_j}$) are written as:

$$Q_\alpha^{mf_i} = CI^{mf_i} \cdot \lambda_\alpha^* \cdot (p^{f_i} - p^m)$$
$$Q_\alpha^{f_i m} = CI^{f_i m} \cdot \lambda_\alpha^* \cdot (p^m - p^{f_i})$$
$$Q_\alpha^{f_i f_j} = CI^{f_i f_j} \cdot \lambda_\alpha^* \cdot (p^{f_j} - p^{f_i}).$$

Here, CI is the so-called connectivity index between each two non-neighboring elements and $CI = \frac{A_{ij}}{\langle d \rangle_{ij}}$. In this formulation, A_{ij} is the area fraction of overlapping fracture elements in the matrix cell and $\#d\#_{ij}$ is the average distance between them [8].

Considering n_α phases in the system, the above equations are written for each phase. As $\sum_{\alpha=1}^{n_\alpha} S_\alpha = 1$ holds, there are in total n_α-*1* number of saturation unknowns and one pressure unknown with n_α number of equations. This article focuses on a two phase problem, with two main unknowns, namely pressure (p) and saturation of phase *1* (S_1).

The system of equations described above is discretized in space using a two-point flux approximation (TPFA) finite volume method (FVM) and is discretized implicitly in time using the backward Euler scheme [21]. Structured grids are imposed on matrix and fractures independently using the projection-based embedded discrete fracture model (pEDFM). The solution to the non-linear fully implicit system is obtained using a Newton-Raphson iterative scheme [21]. The equations are written in residual form.

Let $r^n = \left[(r^m)^n, (r^{f_1})^n, \cdots, (r^{mf_{nfrac}})^n\right]^T$ be the residual vector of the total system at time-step n where $(r^k)^n$ is the residual of the medium k. The residual at time-step $n+1$ is a non-linear function of the main unknowns at the mentioned time-step (i.e., p^{n+1} and S^{n+1}). At each time-step, using Newton–Raphson method, the residual is written as

$$r^{v+1} = r^v + \left.\frac{\partial r}{\partial p}\right|^v \delta p^{v+1} + \left.\frac{\partial r}{\partial S}\right|^v \delta S^{v+1} = 0.$$

The superscript v denotes the iteration index. The linearized system can be written in compact form, i.e., $J^v \times \delta x^{v+1} = -r^v$, where $\boldsymbol{J}^v$ is the Jacobian matrix that consists of sub-blocks and contains all the derivatives. The linear system of equations can be shown as

$$\begin{bmatrix} J^{mm}_{p,p} & J^{mf}_{p,p} & J^{mm}_{p,S} & J^{mf}_{p,S} \\ J^{fm}_{p,p} & J^{ff}_{p,p} & J^{fm}_{p,S} & J^{ff}_{p,S} \\ J^{mm}_{S,p} & J^{mf}_{S,p} & J^{mm}_{S,S} & J^{mf}_{S,S} \\ J^{fm}_{S,p} & J^{ff}_{S,p} & J^{fm}_{S,S} & J^{ff}_{S,S} \end{bmatrix}^{\nu} \times \begin{bmatrix} \delta p^m \\ \delta p^f \\ \delta S^m \\ \delta S^f \end{bmatrix}^{\nu+1} = - \begin{bmatrix} r^m_p \\ r^f_p \\ r^m_S \\ r^f_S \end{bmatrix}^{\nu}$$

The non-linear convergence is achieved by satisfying the following conditions:

$$\frac{||r_p||_2}{||r^0_p||_2} < \epsilon_{rp} \quad , \quad \frac{||r_S||_2}{||r^0_S||_2} < \epsilon_{rS} \quad , \quad ||\delta p||_2 < \epsilon_{\delta p} \quad , \quad ||\delta S||_2 < \epsilon_{\delta S} \ ,$$

where the mentioned conditions are set as user input parameters for the simulator.

Solving such linear systems of equations is computationally challenging, especially for real-field applications and more extensively in presence of coupling terms (e.g., capillarity). In the next section, the algebraic dynamic multilevel (ADM) methodology is explained as an alternative to classical fine-scale simulation addressing the computational challenges involved.

ADM Methodology

The linear system of equation described above is solved using an algebraic dynamic multilevel method. At each time-step, ADM constructs a reduced system algebraically which maps the fine-scale system to a dynamic multilevel grid resolution (i.e., ADM grid). This ADM grid is defined at the beginning of each time-step using a front-tracking technique and error-estimation strategy. At the start of this process, sets of N_m^l and N_f^l hierarchically nested coarse grids are imposed on the matrix and fractures. Here, l denotes the coarsening level and $l=0$ refers to the fine-scale system. The coarsening ratio γ^l is defined as

$$\gamma^l = \left(\gamma^l_m, \quad \gamma^l_{f_1}, \quad \cdots \quad , \quad \gamma^l_{n_{frac}}\right) = \left(\frac{N^{l-1}_m}{N^l_m} \quad , \quad \frac{N^{l-1}_{f_1}}{N^l_{f_1}} \quad , \quad \ldots, \quad \frac{N^{l-1}_{n_{frac}}}{N^l_{n_{frac}}}\right).$$

Due to flexibility of the implementation, the coarsening ratios can be defined independently for each medium. The mapping procedure from fine-scale to ADM grid uses sequences of ADM restriction ($\widehat{R}$) and prolongation ($\widehat{P}$) operators at all coarsening levels. At each iteration, the ADM system reads

$$\underbrace{\hat{R}^{l-1}_l \ldots \quad \hat{R}^0_1 \quad J_0 \quad \hat{P}^1_0 \ldots \quad \hat{P}^l_{l-1} \quad \delta\hat{x}_{ADM}}_{J_{ADM}} = \underbrace{-\hat{R}^{l-1}_l \ldots \quad \hat{R}^0_1 \quad r_0}_{r_{ADM}}$$

In this system, $\hat{R}^{l-1}_l$ is the ADM restriction operator that maps a section of the solution vector from resolution *l-1* to resolution *l*, and $\hat{P}^l_{l-1}$ is the ADM prolongation operator which maps the part of solution vector from *l* to level *l-1*. Once the system is solved at ADM level, the solution (i.e., $\delta\hat{x}_{ADM}$) is mapped to fine-scale resolution as an approximated solution ($\delta x_0'$) using ADM prolongation operators.

$$\delta x_0 \approx \delta x'_0 = \hat{P}^1_0 \ldots \quad \hat{P}^l_{l-1} \quad \delta\hat{x}_{ADM}$$

The ADM operators are assembled from the static multilevel multiscale operators (i.e., R and P) which are constructed on the entire domain for all coarsening levels. The static multilevel prolongation operator reads

$$P_{l-1}^{l}=\begin{pmatrix}\left[(P_p)_{l-1}^{l}\right]_{mm} & \left[(P_p)_{l-1}^{l}\right]_{mf} & & \\ \left[(P_p)_{l-1}^{l}\right]_{fm} & \left[(P_p)_{l-1}^{l}\right]_{ff} & & \\ & & \left[(P_S)_{l-1}^{l}\right]_{mm} & \\ & & & \left[(P_S)_{l-1}^{l}\right]_{ff}\end{pmatrix}_{N_{l-1}\times N_l}.$$

The restriction operator is written as

$$R_l^{l-1}=\begin{pmatrix}\left[R_l^{l-1}\right]_m & & & \\ & \left[R_l^{l-1}\right]_m & & \\ & & \left[R_l^{l-1}\right]_f & \\ & & & \left[R_l^{l-1}\right]_f\end{pmatrix}_{N_l\times N_{l-1}}.$$

To ensure mass conservation on the domain, finite-volume restriction operator is used. In other words,

$$R_l^{l-1}(m,n)=\begin{cases}1 & if\ cell\ n\ is\ inside\ cell\ m\\ 0 & otherwise\end{cases}$$

Different interpolators are used for each of the variables. The prolongation operator for pressure employs multilevel multiscale basis functions. These fully-coupled basis functions are locally computed, taking into account the connectivity of matrix and overlapping fractures. The saturation prolongation operator uses constant basis functions. Therefore, $(P_S)_{l-1}^{l}=[R_l^{l-1}]^T$, with superscript T denoting the transpose operator.

The ADM method uses a user-defined gird selection criterion to obtain the dynamic multilevel resolution map. At each time-step n, the ADM grid resolution is selected based on the information at time-step $n-1$ by using a threshold value set as an input parameter to the simulator at the beginning of simulation. This threshold compares the difference between the values of a parameter (in this work, saturation) inside a grid cell and its neighboring cells in the corresponding coarse node. Therefore, this criterion is based on a spatial gradient. Assuming Ω_l^I and Ω_l^J as the set of two neighboring coarse grid cells I and J at coarsening level l, with grid cell indices i and j at higher resolution (coarsening level $l-1$) belonging to coarse cells I and J, the saturation difference $\Delta\bar{S}_{IJ}$ is calculated as

$$\Delta\bar{S}_{IJ}=\max\left(\left|S_i-S_j\right|\right) \qquad \forall\, i\in\Omega_l^I \qquad and \qquad \forall\, j\in\Omega_l^J .$$

The coarse block I will be refined to level $l-1$ if the condition

$$\Delta\bar{S}_{IN}>tol$$

is met. In this condition, N indicates all the coarse grid cells neighboring the coarse grid cell I. In addition, the grid cell near the wells are always kept at fine-scale resolution ($l=0$) to capture the source term effect accurately.

Numerical Results

Numerical results for two 2D fractured test cases (homogeneous and heterogeneous) are presented in this article. The performance of ADM method is studied and compared to results of fine-scale simulation as reference solution.

The test cases have identical input except the permeability distribution of the rock matrix.

A 2D domain of *100 m×100 m* containing 30 fractures with range of low and high conductivity is considered. Fractures have different lengths, but identical aperture of 5×10^{-3} *[m]*. The rock matrix is discretized to *190×190* Cartesian grids and *534* grids are imposed on the fracture network (in total *36634* grid cells). Four injection wells are located on the left boundary ($P_{inj}=5\times10^{7}$ *[Pa]*) and four production wells exist on the right boundary ($P_{prod}=10^{7}$ *[Pa]*), forming a line-drive well pattern to inject water and produce oil. This means that the wells on each side are located on equidistant intervals. In both test cases the fracture networks consist of *9* high conductive fractures ($K_f=10^{-6}$ *[m²]*) and *21* low conductive fractures ($K_f=10^{-22}$ *[m²]*). Quadratic relative permeability curves are employed using Brooks-Corey formulation. Table 1 shows more details of the input parameters used for these test cases.

Table 1—Input parameters used for both test cases

Property	Value
Rock Porosity	0.2 [-]
Water density	1000 [Kg/m^3]
Oil density	800 [Kg/m^3]
Water viscosity	10^{-3} [*Pa. sec*]
Oil viscosity	3×10^{-3} [*Pa. sec*]
Connate water saturation	0.0 [–]
Residual oil saturation	0.0 [–]

The coarse grid with a maximum of two coarsening levels for the rock matrix and one coarsening level for the fracture network is imposed on the domain. The coarsening ratio in each direction and for each medium is $\gamma=3$. Simulations are run for each test case, including fine-scale and ADM coarsening criterion $\Delta S=0.3$. The ADM results are compared to fine-scale results as reference solution. The error of ADM is calculated as

$$e_x = \frac{||x_{FS} - x_{ADM}||}{||x_{FS}||}$$

where x denotes the main unknowns (i.e., pressure and saturation). ADM and FS subscripts refer to ADM and fine-scale solutions.

Test case 1. In this test case the rock matrix is homogeneous with permeability of $K_m=10^{-14}$ *[m²]*. Simulations are run for *500 [days]* and the results are reported on *100* isochronal time intervals.

Figure 1 and Figure 2 show the fracture network, pressure and saturation plots of fine-scale and ADM simulations related to test case 1. More information such as error value and average percentage of active grid cells used during the simulation is provided under each ADM plot.

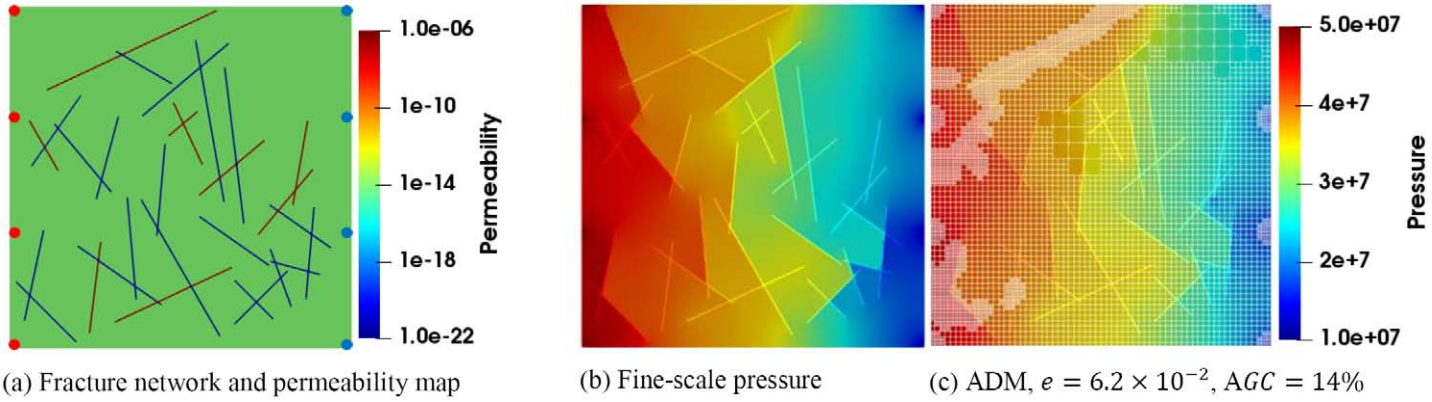

(a) Fracture network and permeability map (b) Fine-scale pressure (c) ADM, $e = 6.2 \times 10^{-2}$, $AGC = 14\%$

Figure 1—Test case1: Pressure plots of fine-scale and ADM simulations. Fig. 1a shows the fracture network and the homogeneous permeability map with fractures permeability range in the color bar. Fig. 1b is the finescale pressure. Fig. 1c is the ADM result (for thresholds ΔS=0.3). Under the ADM plot, error and percentage of active grid cells (AGC) are show.

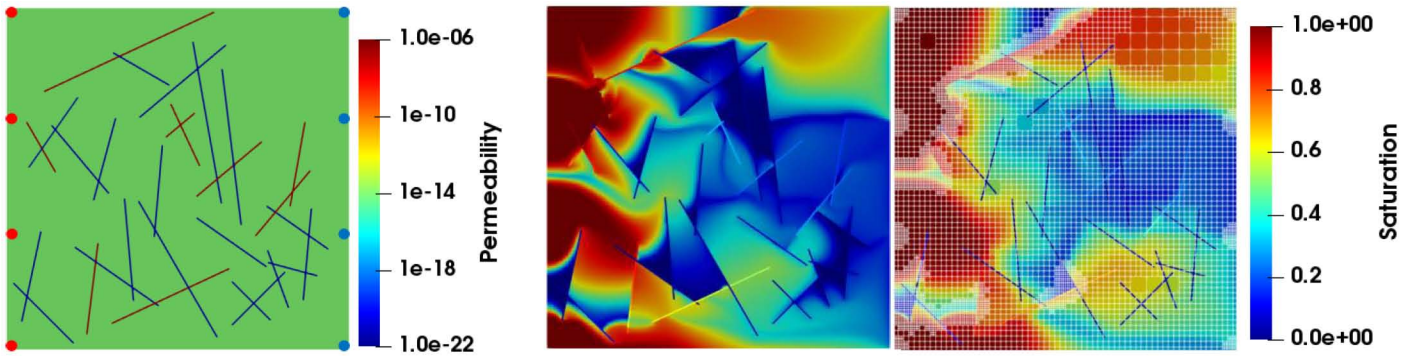

(a) Fracture network and permeability map (b) Fine-scale saturation (c) ADM, $e = 3.1 \times 10^{-1}$, $AGC = 14\%$

Figure 2—Test case 1: Saturation plots of fine-scale and ADM. Similar to Figure 1, the fine-scale solution is compared to ADM result. Error and percentage of active grid cells (AGC) are displayed at bottom of the ADM plot.

It should be mentioned that the ADM keeps the regions around the wells at fine-scale resolution to increase the accuracy and capture the source term effects. As a result, a significant percentage of active grid cells occurs due to this matter, depending on the size of the domain, resolution and number of wells.

Test case 2. This test case contains heterogeneous rock matrix with permeability ranging from min$(K_m)=7.5\times10^{-16}$ $[m^2]$ to max $(K_m)=7.5\times10^{-12}$ $[m^2]$. Note that the heterogeneity contrast in the rock matrix is *4* orders of magnitude. However, including the fractures, this contrast is in *16* orders of magnitude. Simulations are run for 100 *[days]* and the results are reported on *100* isochronal time intervals.

The fracture network, permeability distribution of heterogeneous rock matrix, pressure and saturation plots of fine-scale and ADM simulations related to test case 2 are illustrated on Figure and Figure . Error values and average percentage of active grid cells used during the simulation are given under the ADM plots.

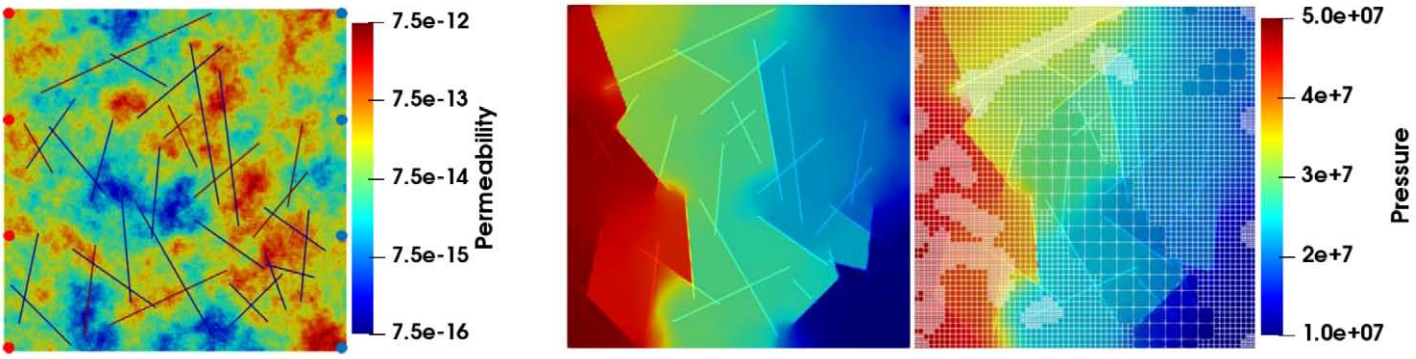

Figure 3—Test case 2: Pressure plots. Fig. 3a shows the fracture network and the hetergoeneous permeability map. Please note that the colorbar only shows the matrix permeability range and fracture networks are identical in both test cases. Fig. 3b is the finescale pressure. Fig. 3c plots the ADM result.

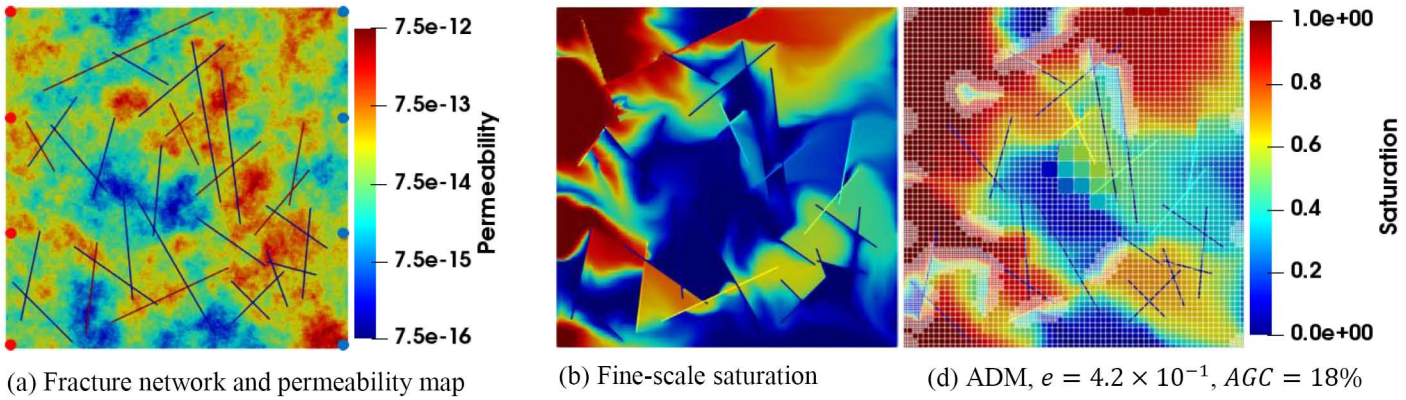

Figure 4—Test case 2: Saturation plots of fine-scale (Fig. 4b) and ADM (Fig. 4c). Fig. 4a shows the fracture network and the hetergoeneous permeability map. Please note that the colorbar only shows the matrix permeability range and fracture networks are identical in both test cases.

Conclusion

An algebraic dynamic multilevel (ADM) method for fully implicit simulation of multiphase flow in fractured porous media using the projection-based embedded discrete fracture model (pEDFM) is presented. The discretized fine-scale fully implicit system with computational grids (imposed on rock matrix and fractures independently using pEDFM) is mapped into a dynamic multilevel resolution grid (i.e., ADM grid). The mapping process is done using sequences of ADM restriction and prolongation operators which are assembled from the static multilevel multiscale operators. The static operators are computed only at the beginning of the simulation once the coarse grids for both matrix and fractures are constructed on all coarsening levels. Locally computed basis functions are used for this purpose. Different interpolators are employed for pressure and saturation. While constant basis functions are used for saturation unknowns, fully coupled multiscale basis functions are computed and employed for pressure unknowns.

The results of two 2D test cases (one with homogeneous and one with heterogeneous rock matrix) containing heterogeneous fracture networks with significant heterogeneity contrasts (*16* orders of magnitude) are shown. The ADM results are compared to fine-scale results as reference solution. The ADM grid is able to dynamically capture the sharp gradients of solution especially at the moving front. Low threshold (high sensitivity to solution gradient) results in employment of higher percentage of active grid cells to capture the front more accurately and therefore decreases the error. However, the performance is compromised due to low threshold. As the threshold increases (i.e., sensitivity decreases) lower active grid cell percentage is used to capture the front, resulting in an increase in ADM error. Please note that in

presence of high heterogeneity contrasts, the percentage of active grid cells increases. Additionally, the error is higher for the heterogeneous test case. In the regions where high conductive and low conductive fractures intersect, due to significant contrast, the simulator struggles to capture the front and provide the solution accurately. However, it can be seen that ADM is able to provide acceptable accuracy by employing only a fraction of fine-scale grid cells, resulting in a reduced system with a smaller number of degrees of freedom (DOF). A detailed sensitivity study and error analysis of ADM performance will be presented in future works. Evidently, one can note that due to the scalability of ADM method, for larger domain, lower fraction of active grid cells will be employed, providing a robust performance compared to fine-scale simulation. Therefore, ADM casts a promising strategy and applicability, especially for real-field scale domains.

Acknowledgement

The authors thank the members of the Delft Advanced Reservoir Simulation (DARSim) research team for the scientific input and worthwhile discussions during the development of this method.

References

1. B. Berkowitz, "Characterizing flow and transport in fractured geological media: A review," *Adv. Water Resour.*, vol. **25**, no. 8–12, pp. 861–884, 2002.
2. T. Praditia, R. Helmig, and H. Hajibeygi, "Multiscale formulation for couple," *Comput. Geo.*, vol. **(in press)**, p. DOI: 10.1007/s10596-018-9754-4, 2018.
3. E. Rossi, M. A. Kant, C. Madonna, M. O. Saar, and P. R. von Rohr, "The Effects of High Heating Rate and High Temperature on the Rock Strength: Feasibility Study of a Thermally Assisted Drilling Method," *Rock Mech. Rock Eng.*, 2018.
4. T. T. Garipov, M. Karimi-Fard, and H. A. Tchelepi, "Discrete fracture model for coupled flow and geomechanics," *Comput. Geosci.*, vol. **20**, no. 1, pp. 149–160, Feb. 2016.
5. L. S. K. Fung and A. H. Dogru, "Parallel Unstructered Solver Methods for Complex Giant Reservoir Simulation," SPE Pap. 106237, SPE Reserv. Simul. Symp. Houston, Texas, USA, 2007.
6. S. H. Lee, C. L. Jensen, and M. F. Lough, "An Efficient Finite Difference Model For Flow In a Reservoir With Multiple Length-Scale Fractures," *SPE ATCE*, Oct. 1999.
7. L. Li and S. H. Lee, "Efficient field-scale simulation of black oil in naturally fractured reservoir through discrete fracture networks and homogenized media," *SPE Reserv. Eval. Eng.*, pp. 750–758, 2008.
8. H. Hajibeygi, D. Karvounis, and P. Jenny, "A hierarchical fracture model for the iterative multiscale finite volume method," *J. Comput. Phys.*, vol. **230**, no. 24, pp. 8729–8743, 2011.
9. M. Tene, S. B. M. Bosma, M. S. Al Kobaisi, and H. Hajibeygi, "Projection-based Embedded Discrete Fracture Model (pEDFM)," *Adv. Water Resour.*, vol. **105**, pp. 205–216, 2017.
10. M. Cusini, C. van Kruijsdijk, and H. Hajibeygi, "Algebraic dynamic multilevel (ADM) method for fully implicit simulations of multiphase flow in porous media," *J. Comput. Phys.*, vol. **314**, pp. 60–79, 2016.
11. M. Cusini, B. Fryer, C. van Kruijsdijk, and H. Hajibeygi, "Algebraic dynamic multilevel method for compositional flow in heterogeneous porous media," *J. Comput. Phys.*, vol. **354**, pp. 593–612, 2018.
12. M. HosseiniMehr, M. Cusini, C. Vuik, and H. Hajibeygi, "Algebraic dynamic multilevel method for embedded discrete fracture model (F-ADM)," *J. Comput. Phys.*, vol. **373**, pp. 324–345, 2018.
13. T. Y. Hou and X.-H. Wu, "A multiscale finite element method for elliptic problems in composite materials and porous media," *J. Comput. Phys.*, vol. **134**, pp. 169–189, 1997.

14. P. Jenny, S. H. Lee, and H. A. Tchelepi, "Multi-scale finite-volume method for elliptic problems in subsurface flow simulation," *J. Comput. Phys.*, vol. **187**, pp. 47–67, 2003.
15. H. Hajibeygi, G. Bonfigli, M. A. Hesse, and P. Jenny, "Iterative multiscale finite-volume method," *J. Comput. Phys.*, vol. **227**, no. 19, pp. 8604–8621, 2008.
16. Y. Wang, H. Hajibeygi, and H. A. Tchelepi, "Monotone Multiscale Finite Volume Method," *Comput. Geosci.*, pp. 1–16, 2015.
17. M. Tene, Y. Wang, and H. Hajibeygi, "Adaptive algebraic multiscale solver for compressible flow in heterogeneous porous media," *J. Comp. Phys.*, vol. **300**, pp. 679–694, 2015.
18. S. B. M. Bosma, H. Hajibeygi, M. Tene, H. A. Tchelepi, and others, "Multiscale Finite Volume Method for Discrete Fracture Modeling with Unstructured Grids," in SPE Reservoir Simulation Conference, 2017.
19. N. Castelletto, S. Klevtsov, H. Hajibeygi, and H. A. Tchelepi, "Multiscale two-stage solver for Biot's poroelasticity equations in subsurface media," *Comput. Geosci.*, vol. **23**, no. 2, pp. 207–224, 2019.
20. I. Sokolova, M. G. Bastisya, and H. Hajibeygi, "Multiscale finite volume method for finite-volume-based simulation of poroelasticity," *J. Comput. Phys.*, vol. **379**, pp. 309–324, 2019.
21. K. Aziz and A. Settari, *Petroleum Reservoir Simulation*. Blitzprint Ltd., Calgary, Alberta, 2002.